

# Interfacial Interactions Between Inclusions Comprising $\text{TiO}_2$ or $\text{TiN}$ and the Mold Flux During the Casting of Titanium-Stabilized Stainless Steel



LEJUN ZHOU, ZIHANG PAN, WANLIN WANG, JUNYU CHEN, LIWEN XUE, TONGSHENG ZHANG, and LEI ZHANG

Interfacial properties play a key role in determining the solubility of solids in liquids for both low- and high-temperature processes. In this study, the interfacial interactions between inclusions comprising  $\text{TiO}_2$  or  $\text{TiN}$  and the mold flux were investigated. The results of sessile drop tests show that the wettability of the mold flux on the  $\text{TiO}_2$  substrate was better than that on the  $\text{TiN}$  substrate when the temperature was below 1503 K. However, the contact angle on the  $\text{TiN}$  substrate decreased more than that on the  $\text{TiO}_2$  substrate when the temperature was above 1503 K due to the enhancement of the interfacial reaction. The thermodynamic calculations suggest that the reactions of  $\text{TiN}$  with  $\text{O}_2$  and  $\text{SiO}_2$  resulted in a bubbling phenomenon during the  $\text{TiN}$  sessile drop test. The scanning electron microscopy (SEM) and energy dispersive spectroscopy (EDS) results show that the final products of the interfacial interaction between the mold flux and the  $\text{TiO}_2$  substrate comprised perovskites, whereas those for the  $\text{TiN}$  substrate comprised perovskites and  $\text{SiTi}$ .

<https://doi.org/10.1007/s11663-019-01746-2>

© The Minerals, Metals & Materials Society and ASM International 2019

## I. INTRODUCTION

BOTH  $\text{TiO}_2$  and  $\text{TiN}$  inclusions are formed during the continuous casting of titanium-stabilized stainless steels since titanium reacts with oxygen and nitrogen from the air, molten steel, or molten slag.<sup>[1–3]</sup> These titanium-based inclusions may deteriorate the surface quality<sup>[4,5]</sup> and the mechanical properties of the stainless steel<sup>[6–8]</sup> if they become entrapped by the solidified shell in the mold. Therefore, the assimilation of the  $\text{TiO}_2$  and  $\text{TiN}$  inclusions liberated from the molten steel by the liquid mold flux is important for their control or removal during the casting process.

The effect of the  $\text{TiO}_2$  and  $\text{TiN}$  contents on the properties of the slag, such as its viscosity and crystallization,<sup>[9–12]</sup> has been studied intensively; however, investigations on the dissolution behavior of  $\text{TiO}_2$  and  $\text{TiN}$  in molten slag are relatively few. Sharma *et al.*<sup>[13]</sup> studied the dissolution kinetics of  $\text{TiO}_2$  inclusions in

steelmaking slags using high-temperature confocal scanning laser microscopy, and the results suggest that the dissolution rate of the  $\text{TiO}_2$  in the slag might be controlled by a chemical reaction. Ren *et al.*<sup>[14]</sup> conducted experiments on the dissolution of  $\text{TiO}_2$  in a  $\text{CaO-Al}_2\text{O}_3\text{-SiO}_2$  slag at temperatures ranging from 1643 K to 1073 K (1370 °C to 800 °C) and found that the dissolution was enhanced at high temperatures but restrained by the  $\text{Al}_2\text{O}_3$  content. Moreover, Ozturk<sup>[15]</sup> investigated the solubility of  $\text{TiN}$  in continuous casting powders through a slag-nitride equilibration technique and found that the solubility of the  $\text{TiN}$  increased with increasing  $\text{SiO}_2$  content. Similar results obtained by Michelic *et al.*<sup>[16]</sup> also indicated that slags with elevated  $\text{SiO}_2$  content showed a significantly increased ability to dissolve  $\text{TiN}$  compared to that of  $\text{Al}_2\text{O}_3$  rich slags.

Although several relevant works have been performed, most of them focused on the variation of the solubility with the slag composition; very few of them involved the interfacial interaction between the inclusions comprising  $\text{TiO}_2$  or  $\text{TiN}$  and the mold flux. In fact, the assimilation of these inclusions depends greatly on the interfacial wetting ability of the liquid mold flux on the solid inclusions, since wetting the inclusions is the first step to dissolve them. Therefore, the interfacial interactions between the mold flux droplet and inclusions comprising  $\text{TiO}_2$  or  $\text{TiN}$  were studied in this paper. The spreading behavior and contact angle variation of the mold flux droplet on substrates comprising the same

LEJUN ZHOU, ZIHANG PAN, WANLIN WANG, JUNYU CHEN, LIWEN XUE, TONGSHENG ZHANG, and LEI ZHANG are with the School of Metallurgy and Environment, Central South University, Changsha 410083, China and also with the National Center for International Research of Clean Metallurgy, Central South University, Changsha 410083, China. Contact e-mail: wanlin.wang@gmail.com

Manuscript submitted August 5, 2019.

Article published online December 4, 2019.

material as the inclusions, the thermodynamics of the interfacial reactions, and the microstructure together with the element distribution in the vicinity of the interface were investigated. The goal was to clarify the interfacial mechanism of the dissolution of the TiO<sub>2</sub> and TiN inclusions in the mold flux and then provide guidance for the control or removal of inclusions during the continuous casting of titanium-stabilized stainless steel.

## II. EXPERIMENTAL PROCEDURES

### A. Sample Preparation

The chemical composition of the mold flux used in this study is listed in Table I. The flux was first prepared by mixing CaCO<sub>3</sub>, SiO<sub>2</sub>, Al<sub>2</sub>O<sub>3</sub>, MgO, Na<sub>2</sub>CO<sub>3</sub>, and CaF<sub>2</sub> chemical reagents in a stirrer. Then, the mixture was melted in an induction furnace for 30 minutes to eliminate bubbles and homogenize its chemical compositions. Next, the molten slag was quenched on a water-cooled copper plate to obtain a fully glassy phase. The final samples for the sessile drop test were obtained from the glassy mold flux by grinding it into cubes with an edge length of 5 mm. In addition, the chemical composition of the mold flux after premelting was also analyzed using X-ray fluorescence (XRF; S4 Pioneer, Bruker AXS, Karlsruhe), inductively coupled plasma optical emission spectroscopy (ICP-OES; SPECTRO-BLUE, SPECTRO Corporation), and the ion-selective electrode method (ISE; PF-2-01, Shanghai LEICI Corporation). The analysis results suggest that the volatilization loss of components in the mold flux was very small and could be ignored, as shown in Table I.

The original TiN and TiO<sub>2</sub> substrates were purchased from HeFei Crystal Technical Material Corporation, and their components were confirmed by X-ray diffraction (XRD; RIGAKU-TTR III, Rigaku Corporation), as shown in Figure 1. To eliminate the influence of the surface roughness on the interface properties, both the TiN and TiO<sub>2</sub> substrates were polished with SiC sandpaper with a grit size down to 2000 mesh. The surface roughness of these substrates after polishing was further measured by laser confocal microscopy (V12000DX, Lasertec Corporation). As shown in Figure 2, the surface morphology of these substrates was very similar, and the average roughness of the TiO<sub>2</sub> and TiN substrates was 3.094 and 3.125 μm, respectively, which suggests that its influence could also be ignored.

### B. Sessile Drop Test

The experiments related to the interfacial interaction between the mold flux and the TiO<sub>2</sub> and TiN substrates were mainly carried out by a sessile drop apparatus. A schematic of the apparatus is shown in Figure 3.<sup>[17]</sup> The cube-shaped slag sample was placed on top of the TiO<sub>2</sub> and TiN substrates (Figure 4) and placed into the center of a high-purity alumina reaction tube. Then, the sample was heated at 5 K/min by silicon carbide heating elements and held at 1773 K (1500 °C) for 30 minutes. The holding temperature was chosen to be 1773 K (1500 °C) because it is close to the temperature at the interface between the molten steel and liquid mold flux in molds during the titanium-stabilized stainless steel casting process. To control the atmosphere inside the furnace, high-purity argon gas was first deoxidized and denitrified by slowly passing through a gas purifier at 673 K to 1073 K (400 °C to 800 °C) and then it flowed into the furnace at a flow rate of 300 mL/min. The deoxidizer and denitrifier in the gas purifier were Cu, Al, and Mg, for example. The partial pressure of oxygen (PO<sub>2</sub>) and partial pressure of nitrogen (PN<sub>2</sub>) at the exit of the furnace were detected to be approximately 1 × 10<sup>-18</sup> and 1 × 10<sup>-6</sup> atm, respectively, by the oxygen and nitrogen monitor systems (MOT500-M, Korno Company).

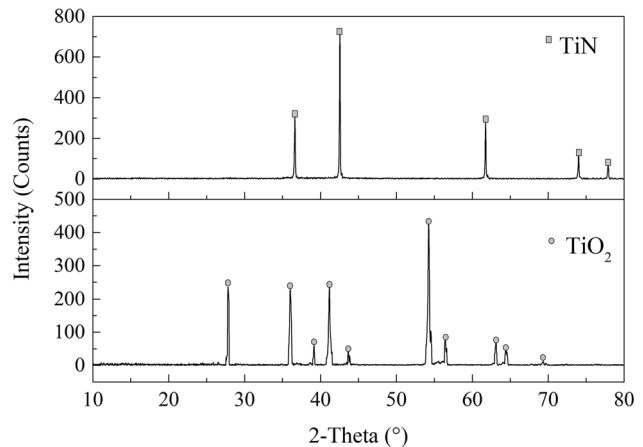


Fig. 1—X-ray diffraction patterns of the TiO<sub>2</sub> and TiN substrates.

Table I. Composition of the Slag Used in This Study (Weight Percent)

	Basicity	CaO	SiO <sub>2</sub>	Al <sub>2</sub> O <sub>3</sub>	Na <sub>2</sub> O	F <sup>-</sup>	MgO
Before pre-melting	1.10	39.81	36.19	6.00	9.00	7.00	2.00
After pre-melting	1.11	40.06	36.02	6.03	8.96	6.92	2.01

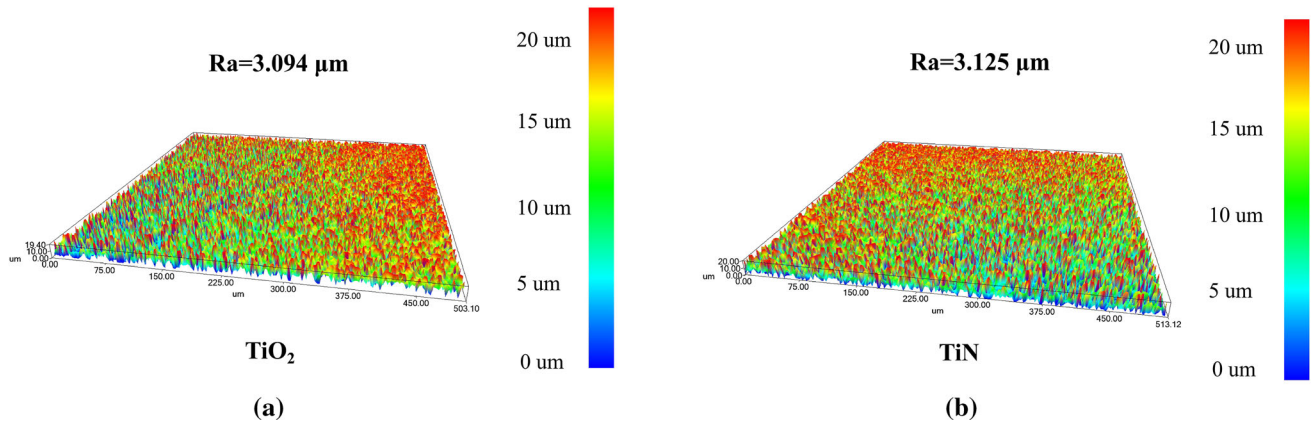


Fig. 2—Surface roughness of the substrates: (a)  $\text{TiO}_2$  and (b) TiN.

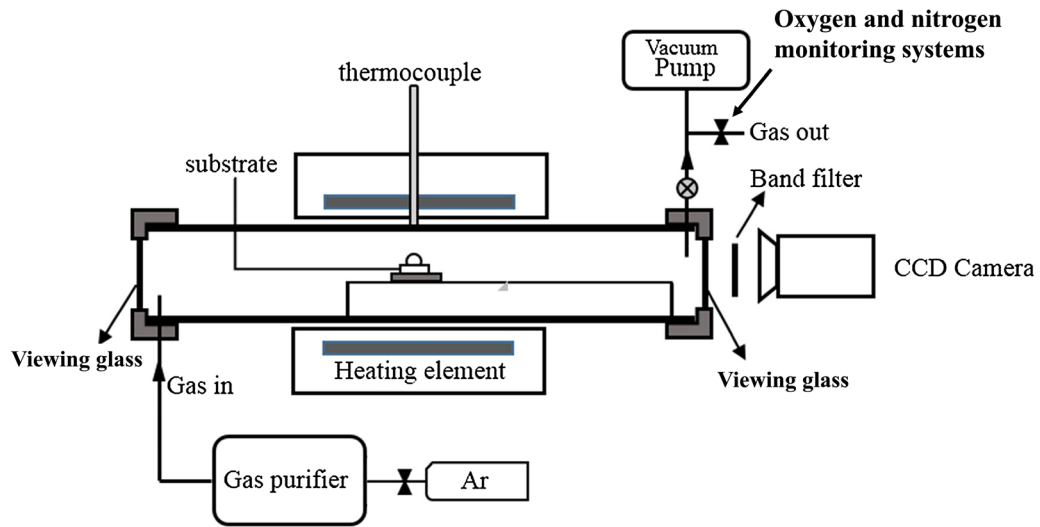


Fig. 3—Schematic figure of the sessile drop apparatus.

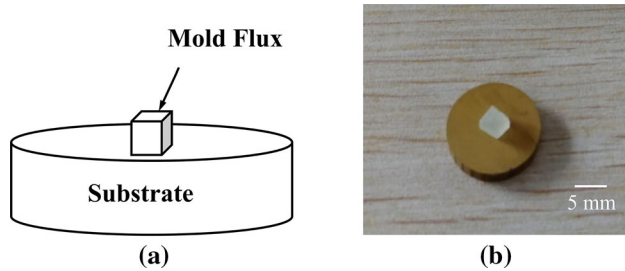


Fig. 4—The mold flux sample on the substrate: (a) a schematic and (b) photograph of the real sample.

The spreading behavior of the mold flux on the  $\text{TiO}_2$  and TiN substrates during the whole test was recorded by a CCD camera. The contact angle was obtained with the ImageJ software package (Version 1.48, National Institutes of Health). Furthermore, after the sessile drop test, both the mold flux and substrate were sampled to

observe the micromorphology and element distribution in the vicinity of the interface by scanning electron microscopy (SEM; JSM-6360LV, Japanese Electronics Company) and energy dispersive spectroscopy (EDS; EDX-GENESIS 60S, America EDAX Corporation).

### III. RESULTS AND DISCUSSION

#### A. Spreading Behavior of the Mold Flux on the Substrates

The preset heating curve and snapshots of the spreading of the mold flux on the  $\text{TiO}_2$  substrate during the sessile drop test are shown in Figure 5. The whole process can be divided into three stages according to the change in the profile of the mold flux sample. In stage I, the mold flux retained its cubic shape on the substrate due to the low temperature that ranged from 273 K to 1473 K (0 °C to 1200 °C). When the temperature reached 1473 K (1200 °C), the shape of the mold flux

started to deform since it began to melt in stage II. The bottom of the mold flux increased with increasing temperature under the effect of gravity. At the end of stage II, the mold flux became fully liquid, and its shape became hemispherical at 1503 K (1230 °C) due to the surface and interfacial tension effects. The mold flux droplet spread continuously on the TiO<sub>2</sub> substrate with a further increase in the temperature from 1503 K to 1773 K (1230 °C to 1500 °C) in stage III, which suggests that the mold flux had good wettability on the TiO<sub>2</sub> substrate.

The spreading behavior of the mold flux on the TiN substrate was similar to that on the TiO<sub>2</sub> substrate during the first two stages of the test; however, a difference occurred in stage III. Figure 6 shows snapshots of the spreading of the mold flux on both the TiO<sub>2</sub> and TiN substrates in stage III. The profile of the mold flux droplet on the TiO<sub>2</sub> substrate was always smooth, although the contact angle decreased with increasing temperature, whereas the profile of the mold flux droplet on the TiN substrate was uneven when the temperature increased. Bubbles formed on the molten mold flux on the TiN substrate, which caused fluctuations on the surface of the mold flux droplet. The details concerning this phenomenon are discussed in Section III-B.

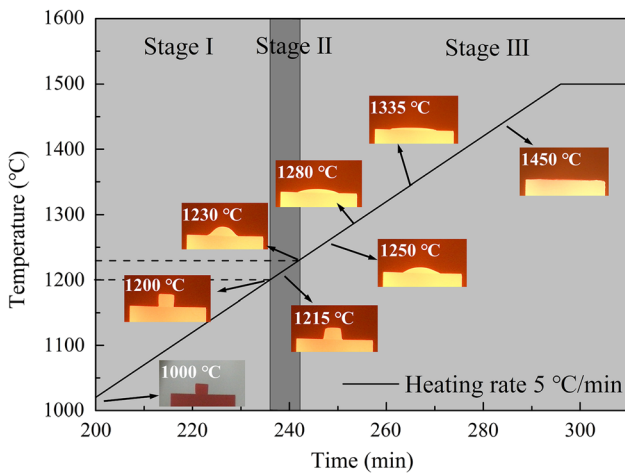


Fig. 5—The preset heating curve and snapshots of the spreading of the mold flux on the TiO<sub>2</sub> substrate.

### B. Variation of the Contact Angle

The contact angle between the mold flux and the substrates at different temperatures was obtained with the ImageJ software package and is shown in Figure 7. The contact angle of both TiO<sub>2</sub> and TiN substrates was 90° when the temperature was low, and the mold flux was in the solid state. It dropped sharply due to the melting of mold flux when the temperature was greater than 1473 K (1200 °C). In stage II, the contact angle between the mold flux and the TiN substrate was slightly larger than that of the TiO<sub>2</sub> substrate at the end of the melting stage. These results indicate that the wettability of the mold flux on the TiO<sub>2</sub> substrate was better than that on the TiN substrate if the interfacial reaction was weak and the temperature was low. In stage III, the contact angle between the mold flux and the TiN substrate dropped below that of the TiO<sub>2</sub> substrate due to an enhancement in the interfacial reaction between the mold flux and the TiN substrate.

To explore the reasons why bubbles formed and the contact angle varied, the thermodynamics of the interfacial reactions between the mold flux and substrates comprising TiO<sub>2</sub> and TiN were calculated with FactSage (Version 7.2, Thermfact and GTT Technologies Company). Table II shows the possible reactions (1) through (14) between the components of the mold flux and substrates comprising TiO<sub>2</sub> and TiN. The Gibbs free

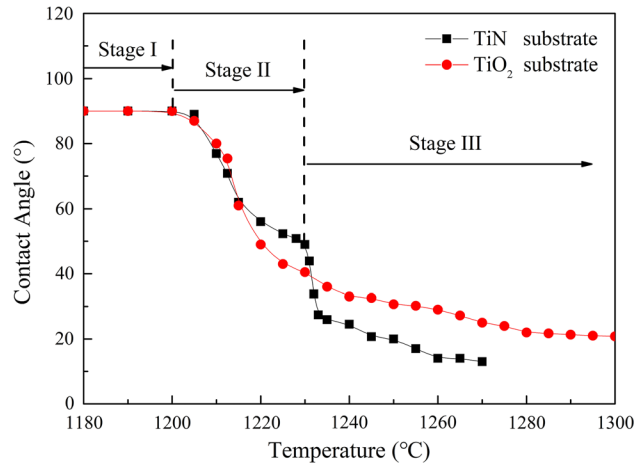


Fig. 7—The contact angle between the mold flux and substrates at different temperatures.

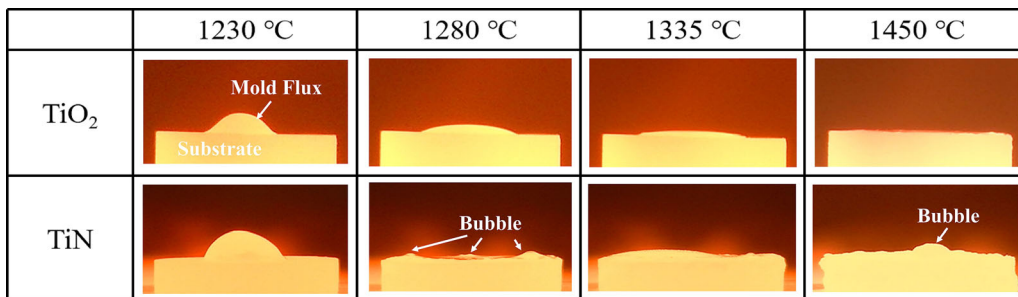


Fig. 6—The spreading of the mold flux droplet on the TiO<sub>2</sub> and TiN substrates.

**Table II. The Possible Reactions Between Slag Components and Substrates**

Substrate	Reaction	
TiN	$2\text{TiN} + 2\text{SiO}_2 = 2\text{SiTi} + 2\text{O}_2\uparrow + \text{N}_2\uparrow$	(1)
	$2\text{TiN} + 2\text{O}_2 = 2\text{TiO}_2 + \text{N}_2\uparrow$	(2)
	$2\text{TiN} + 2\text{SiO}_2 = 2\text{TiO}_2 + 2\text{Si}\uparrow + \text{N}_2\uparrow$	(3)
	$4\text{TiN} + 6\text{CaO} + \text{O}_2 = 4\text{TiO}_2 + 2\text{Ca}_3\text{N}_2$	(4)
	$4\text{TiN} + 6\text{MgO} + \text{O}_2 = 4\text{TiO}_2 + 2\text{Mg}_3\text{N}_2$	(5)
	$2\text{TiN} + 6\text{Na}_2\text{O} + \text{O}_2 = 2\text{TiO}_2 + 2\text{Na}_3\text{N}$	(6)
	$4\text{TiN} + 2\text{Al}_2\text{O}_3 + \text{O}_2 = 4\text{TiO}_2 + 4\text{AlN}$	(7)
	$2\text{TiN} + 3\text{CaF}_2 = 2\text{TiF}_2 + \text{Ca}_3\text{N}_2 + \text{F}_2\uparrow$	(8)
TiO <sub>2</sub>	$\text{TiO}_2 + \text{CaO} = \text{CaTiO}_3$	(9)
	$\text{TiO}_2 + \text{MgO} = \text{MgTiO}_3$	(10)
	$\text{TiO}_2 + \text{Na}_2\text{O} = \text{Na}_2\text{TiO}_3$	(11)
	$8\text{TiO}_2 + 6\text{Al}_2\text{O}_3 = \text{Al}_2\text{TiO}_5$	(12)
	$\text{TiO}_2 + \text{SiO}_2 = \text{TiSiO}_3$	(13)
	$\text{TiO}_2 + \text{CaF}_2 = \text{CaTiO}_2\text{F}$	(14)

energy change (Delta G) of reactions (1) through (12) in the temperature range from 1473 K to 1773 K (1200 °C to 1500 °C) was calculated and is shown in Figures 8(a) and (b). The Delta G of reactions (13) and (14) in Table II could not be obtained from FactSage due to the lack of basic data for TiSiO<sub>3</sub> and CaTiO<sub>2</sub>F.

Table II and Figure 8(a) show that TiN reacted with O<sub>2</sub> and SiO<sub>2</sub> at the experimental conditions because the lines for reactions (1) and (2) in Figure 8(a) were lower than 0 J/mol. Specifically, the TiN substrate reacted with O<sub>2</sub> below 1641 K (1368 °C), whereas it reacted with SiO<sub>2</sub> from the mold flux above that temperature. However, regardless of whether reaction (1) or reaction (2) occurred, the nitrogen gas formed since the N<sub>2</sub>↑ is one of the products in both reactions. Thus, the formation of nitrogen gas through the interfacial reactions resulted in the bubbling phenomenon that occurred during the TiN substrate sessile drop test, as shown in Figure 6. In fact, the release of nitrogen as a result of the contact between TiN and slag during the steelmaking processes of titanium-stabilized stainless steel has been observed by previous researchers.<sup>[16,18,19]</sup> The contact is always accompanied by the formation of metal-slag conglomerates (crust), which cause issues during the steelmaking processes.<sup>[20,21]</sup> The TiN substrate sessile drop test and the thermodynamic calculations here provide strong evidence that these indeed occur during high-temperature processes.

In addition, from Table II and Figure 8(b), the TiO<sub>2</sub> substrate reacted with CaO, MgO, and Na<sub>2</sub>O from the mold flux, which is also because the lines for reactions (9) and (10) were lower than 0 J/mol. According to these reactions, no gas product was formed. Therefore, no bubbles were observed during the sessile drop test when the TiO<sub>2</sub> substrate was used. Furthermore, the mold flux had better wettability on both the TiO<sub>2</sub> and TiN substrates than that on the pure iron or steel substrates, as investigated in our previous papers.<sup>[22,23]</sup> These very intense chemical reactions that occurred at the interface between the mold flux and substrates comprising TiO<sub>2</sub> and TiN caused the improved wettability. The element and electrical charge transport during these reactions

greatly lowered the interfacial tension and enhanced the wettability of the mold flux on the TiO<sub>2</sub> and TiN substrates.

### C. Microstructure and Element Distribution in the Vicinity of the Interface

The microstructure and element distribution at the interface between the mold flux droplet and substrates after the sessile drop test were analyzed by SEM and EDS, and the results are shown in Figures 9, 10, and 11. Among these, Figures 9(a) and (c) show the top view of the mold flux and substrates, and Figures 9(b) and (d) show the cross-sectional profiles of the samples. A comparison of Figures 9(a) and (c) shows that the mold flux gathered in the middle of the TiO<sub>2</sub> substrate, whereas it covered the whole top face of the TiN substrate. The mold flux on both substrates transformed into an opaque color, which might be due to the precipitation of crystals or other high melting point components. In addition, holes were found on the mold flux side of the cross-sectional profile of the TiN substrate, as shown in Figure 9(d), but no holes were found in the cross-sectional profile of the TiO<sub>2</sub> substrate, as shown in Figure 9(b). These results confirmed the observations that bubbling occurred during the TiN substrate sessile drop test, and no bubbling occurred when the TiO<sub>2</sub> substrate was tested.

To observe the microstructure at the interface between the mold flux and TiO<sub>2</sub> substrate in detail, the boxed zones at positions I and II in Figure 9(b) were magnified and are shown in Figures 10(a) and (b). The left side of Figures 10(a) and (b) shows the TiO<sub>2</sub> substrate, and block crystals were found on the mold flux side. The distribution of the crystals in the mold flux formed a radial pattern from the substrate on the left side to the mold flux on the right side. The size of the crystals that were close to the TiO<sub>2</sub> substrate was generally larger than those far away from the TiO<sub>2</sub> substrate. It seems that TiO<sub>2</sub> was transferred from the substrate to mold flux through a diffusive process. Figures 10(c) through (f) show the EDS results of the

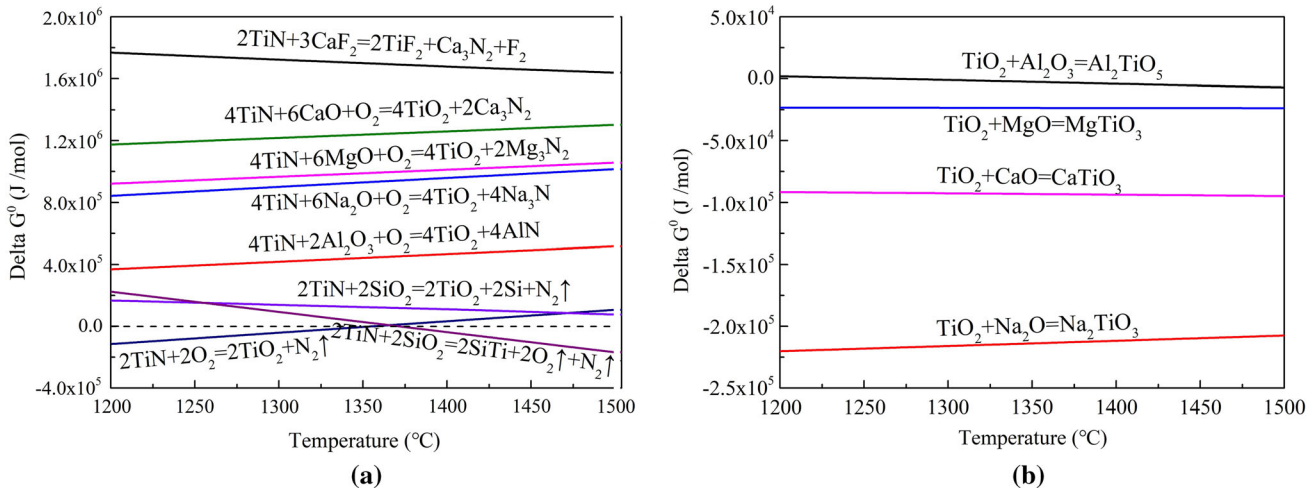


Fig. 8—The variation of the Gibbs free energy change ( $\Delta G$ ) with the temperature at  $\text{PO}_2 = 10^{-18}$  atm and  $\text{PN}_2 = 10^{-6}$  atm on a (a) TiN substrate and (b) TiO<sub>2</sub> substrate.

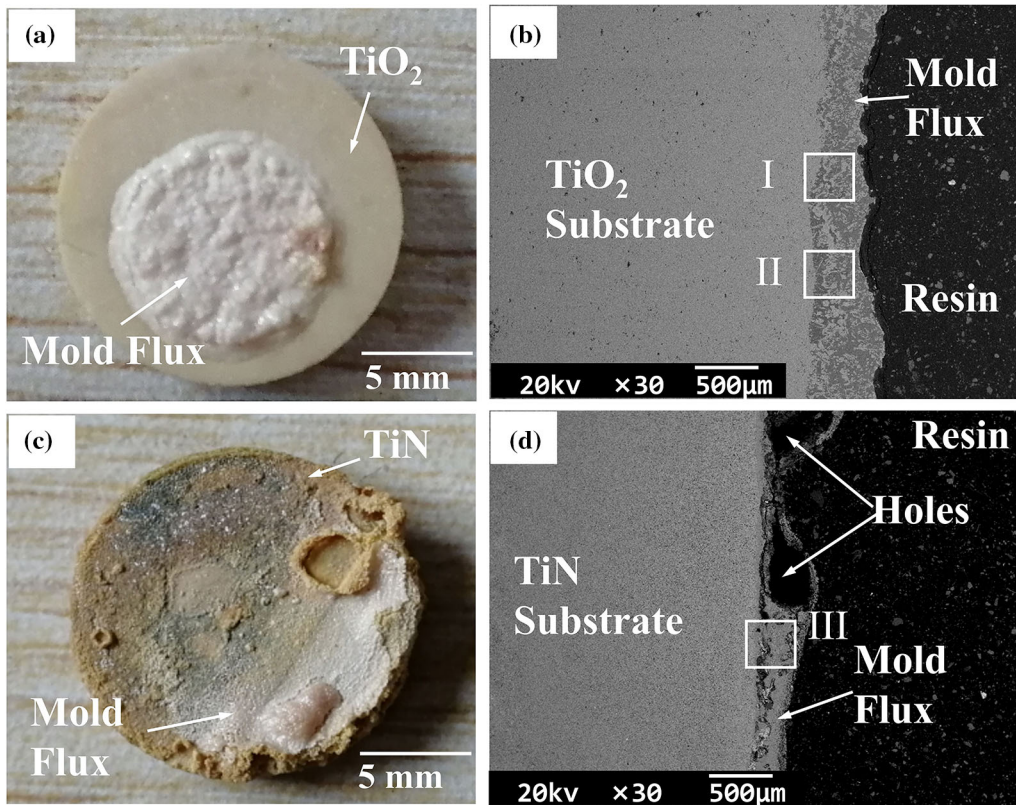


Fig. 9—Top view and cross-sectional profile of the samples after the sessile drop test: (a) top view of the mold flux on the TiO<sub>2</sub> substrate, (b) cross-sectional profile of the mold flux on the TiO<sub>2</sub> substrate, (c) top view of the mold flux on the TiN substrate, and (d) cross-sectional profile of the mold flux on the TiN substrate.

points in Figures 10(a) and (b). The EDS of points A and B suggests that the dark area in Figures 10(a) and (b) was mainly composed of mold flux since Na, Mg, Al, Si, and Ca were components of the mold flux. The content of Ti at point A was 11.43 wt pct, which was higher than the 3.52 wt pct value at point B; on the contrary, the Ca contained at point A was less than that

at point B. These results show that TiO<sub>2</sub> did diffuse from the substrate to the mold flux, but the components in the mold flux diffused in the opposite direction. In addition, the EDS results of points C and D show that the main components of the crystals were O, Ca and Ti; Na was not found, which indicates that the crystals were perovskite (CaTiO<sub>3</sub>) rather than Na<sub>2</sub>TiO<sub>3</sub>. Although

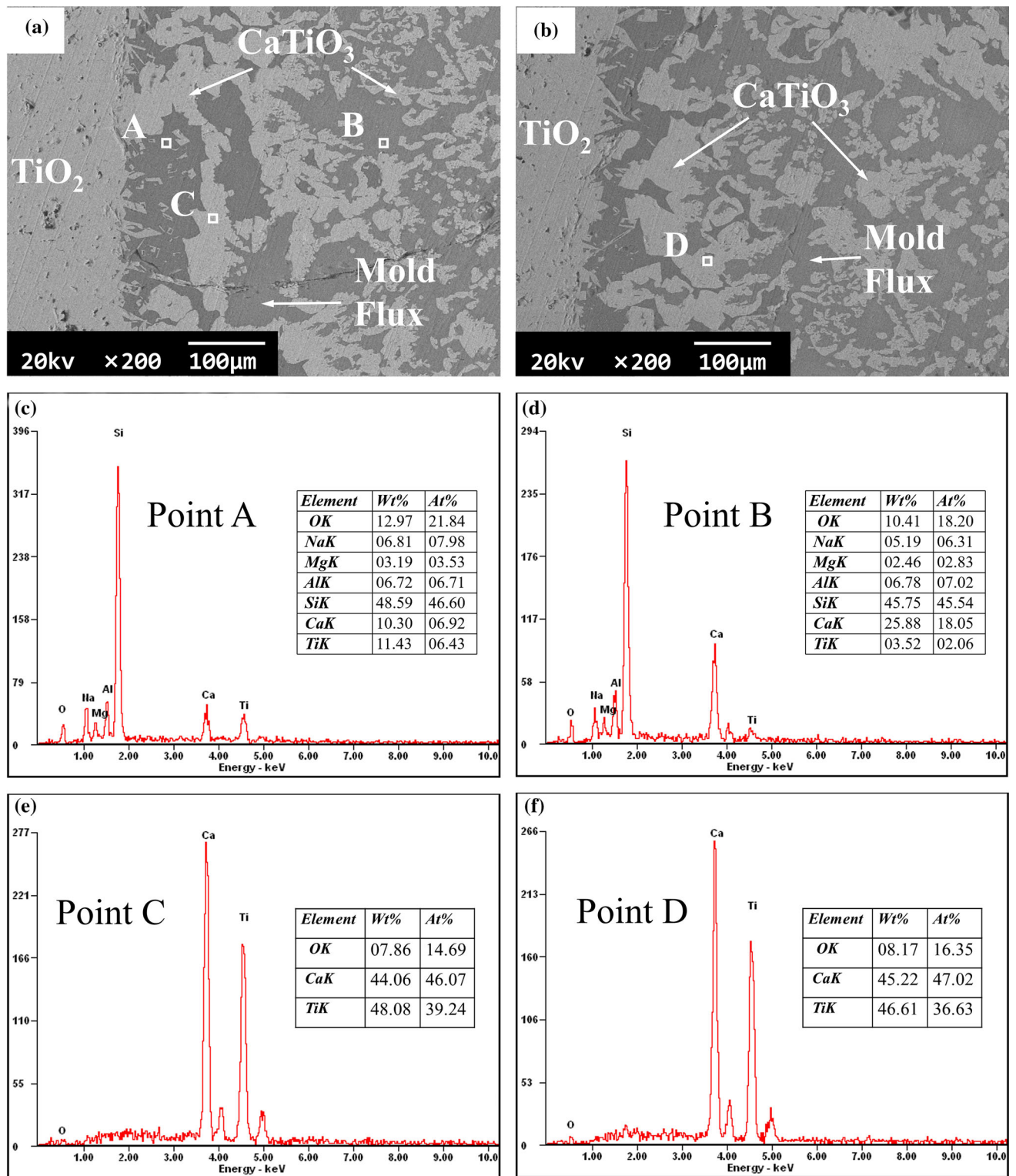
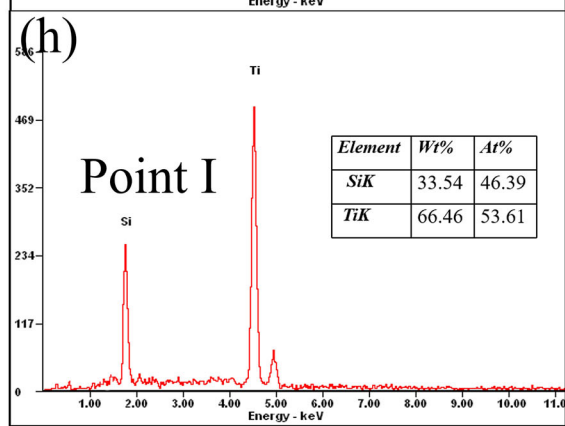
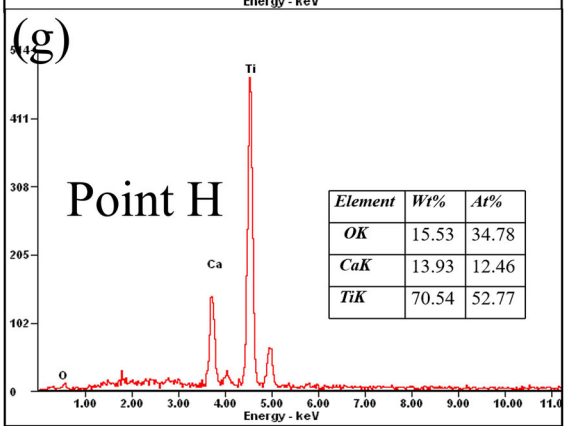
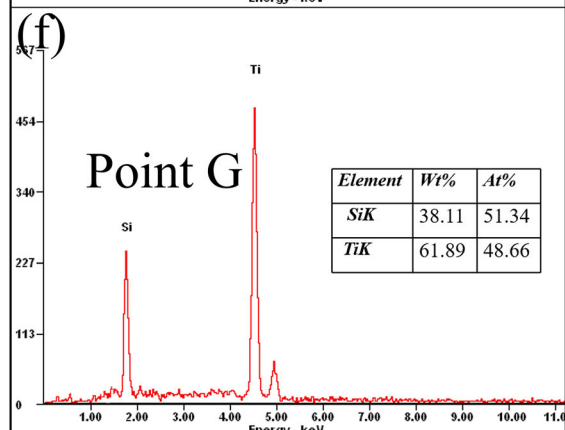
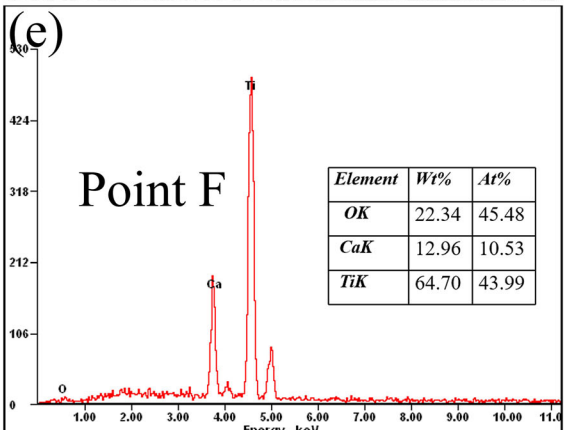
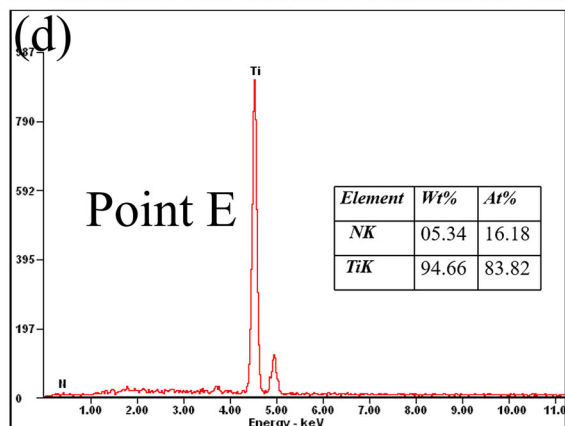
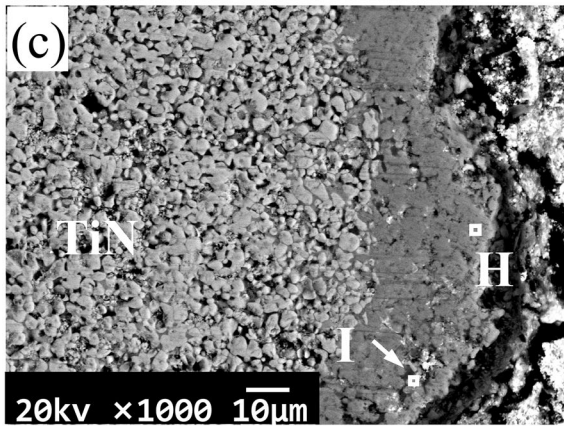
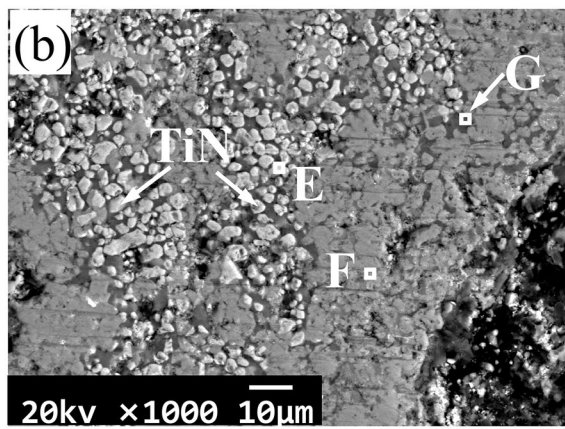
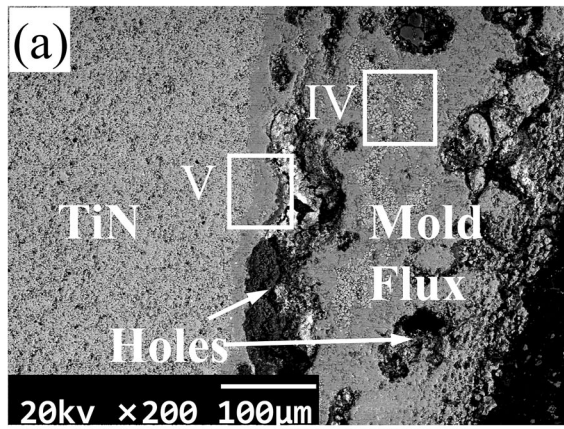


Fig. 10—SEM images and EDS spectra for the labelled positions on the cross-sectional profile of the mold flux on the  $\text{TiO}_2$  substrate: (a) SEM image of position I, (b) SEM image of position II, (c) EDS spectrum of point A, (d) EDS spectrum of point B, (e) EDS spectrum of point C, and (f) EDS spectrum of point D.

$\text{Na}_2\text{TiO}_3$  is more stable than  $\text{CaTiO}_3$  according to Figure 8(b), it precipitated very little since the experimental temperature was 1773 K, which is higher than its melting point 1303 K. Therefore, by combining the

thermodynamic calculations in Figure 8(b) and the SEM and EDS results in Figure 10, it can be concluded that the mechanism of the interfacial interaction between the mold flux and  $\text{TiO}_2$  substrate involved





◀ Fig. 11—SEM images and EDS spectra for the labelled positions on the cross-sectional profile of the mold flux on the TiN substrate: (a) SEM image of position III, (b) SEM image of position IV, (c) SEM image of position V, (d) EDS spectrum of point E, (e) EDS spectrum of point F, (f) EDS spectrum of point G, (g) EDS spectrum of point H, and (h) EDS spectrum of point I.

TiO<sub>2</sub> from the substrate and CaO, MgO, Al<sub>2</sub>O<sub>3</sub> from the mold flux meeting at the interface as a result of the concentration-driven diffusion; the species then reacted to produce perovskites, such as CaTiO<sub>3</sub>.

Figure 11 shows the SEM and EDS results of the interface area between the mold flux and TiN substrate. Among these, Figure 11(a) is a magnified image of the boxed zone at position III in Figure 9(d). The left side of Figure 11(a) shows the TiN substrate, whereas the right side shows the mold flux. Figures 11(b) and (c) are further magnified images of the boxed zones at positions IV and V in Figure 11(a). Position V is closer to the substrate than position IV. Figures 11(b) and (c) show that there were aggregated particles with a light color on the mold flux side, which had a morphology similar to that of the substrate. The EDS results for position E in Figure 11(b) confirmed that these aggregate particles were TiN because they contained characteristic peaks that belong to Ti and N. The existence of aggregate particles in the mold flux suggests that TiN entered the mold flux in a way that was different from that of TiO<sub>2</sub> during the sessile drop tests. The nitrogen bubbles that were produced from the interfacial reactions caused the TiN to detach and float up. The EDS results from point F in Figure 11(b) and point H in Figure 11(c) indicate that the light gray areas in the mold flux were perovskite since the main elements were Ca, Ti, and O. Furthermore, there were still some dark gray areas in Figures 11(b) and (c). The EDS results of points G and point I suggest that their components were Si and Ti. SiTi is a metallic compound with a high melting temperature and is a strong reductant that reacted with the CaO, Na<sub>2</sub>O, MgO, Al<sub>2</sub>O<sub>3</sub>, and SiO<sub>2</sub> in the mold flux, resulting in the gasification and vaporization of these components in the form of Ca↑, Na↑, Mg↑, AlF<sub>3</sub>↑, and SiF<sub>4</sub>↑. Thus, by combining the thermodynamic calculations in Figure 8(a) and the SEM and EDS results in Figure 11, the mechanism of the interfacial interaction between the mold flux and TiN substrate can also be concluded to involve TiN from the substrate detaching and floating up into the molten slag by the action of the nitrogen bubbles. The TiN is then either oxidized into TiO<sub>2</sub> by O<sub>2</sub> that was absorbed and transferred by the molten mold flux at low temperatures or transformed into SiTi by SiO<sub>2</sub> that was contained in the mold flux. Subsequently, part of the SiTi reacted with the components contained in the flux and caused part of the Ca, Mg and Na to be gasified and vaporized and removed from the system, and the oxidative product of TiO<sub>2</sub> further reacted with CaO to form the perovskites.

## IV. CONCLUSIONS

The interfacial interactions between the mold flux droplets and TiO<sub>2</sub> and TiN substrates were investigated in this study. Based on the experimental results and analysis of the spreading behavior, contact angle variation, interfacial reactions, microstructure, and element distribution in the vicinity of the interface between the mold flux and substrates, the following conclusions can be drawn:

- (1) The contact angle decreased sharply with increasing temperature. The contact angle between the mold flux and the TiN substrate decreased more than that of the TiO<sub>2</sub> substrate at temperatures higher than 1503 K (1230 °C) due to the enhancement of the interfacial reaction effect.
- (2) The results of thermodynamic calculations and the SEM and EDS results show that the mechanism of the interfacial interaction between the mold flux and TiO<sub>2</sub> substrate involved TiO<sub>2</sub> from the substrate and CaO, MgO, and Al<sub>2</sub>O<sub>3</sub> from the molten mold flux meeting at the interface through diffusion driven by the concentration gradient and then reacting to produce perovskites, such as CaTiO<sub>3</sub>.
- (3) Moreover, the mechanism of the interfacial interaction between the mold flux and TiN substrate involved TiN from the substrate detaching and floating up into the molten mold flux due to the action of the nitrogen bubbles and then either oxidizing into TiO<sub>2</sub> by the O<sub>2</sub> absorbed and transferred by the mold flux at low temperature or transforming into SiTi by the SiO<sub>2</sub> contained in mold flux. Subsequently, part of SiTi reacted with the components contained in the flux and caused part of Ca, Mg and Na to be gasified and vaporized and removed from the system; the oxidative product TiO<sub>2</sub> then reacted with CaO to form the perovskites.

## ACKNOWLEDGMENTS

This work was supported by the national natural science foundation of China (51874363, U1760202), the Natural Science Foundation of Hunan Province (2019JJ40345), and Hunan Scientific Technology projects (2018RS3022, 2018WK2051).

## REFERENCES

1. B. Ozturk, R. Matway, and R.J. Fruehan: *Metall. Mater. Trans. B*, 1995, vol. 26B, pp. 563–67.
2. Q. Wang, Y.J. Lu, S.P. He, K.C. Mills, and Z.S. Li: *Ironmak. Steelmak.*, 2011, vol. 38, pp. 297–301.
3. J.O. Jo, W.Y. Kim, D.S. Kim, and J.J. Pak: *Met. Mater. Int.*, 2008, vol. 14, pp. 531–37.
4. X. Yin, Y. Sun, Y. Yang, X. Bai, M. Barati, and A. Mclean: *Metall. Mater. Trans. B*, 2016, vol. 47B, pp. 3274–84.
5. D. Kruger and A. Garbers-Craig: *Metall. Mater. Trans. B*, 2017, vol. 48B, pp. 1514–32.
6. J.H. Park and Y. Kang: *Steel. Res. Int.*, 2017, vol. 88, p. 1700130.

7. S. Xu, X.Q. Wu, E.H. Han, W. Ke, and Y. Katada: *Mater. Sci. Eng. A*, 2008, vol. 490, pp. 16–25.
8. M.B. Leban and R. Tisu: *Eng. Fail. Anal.*, 2013, vol. 33, pp. 430–38.
9. H. Park, J.Y. Park, G.H. Kim, and I. Sohn: *Steel Res. Int.*, 2012, vol. 83, pp. 150–56.
10. Z. Wang, Q. Shu, and K. Chou: *Metall. Mater. Trans. B*, 2013, vol. 44, pp. 606–13.
11. J.B. Kim and I. Sohn: *J. Non-Cryst. Solids*, 2013, vol. 379, pp. 235–43.
12. Z. Hao, W. Chen, and C. Lippold: *Metall. Mater. Trans. B*, 2010, vol. 41B, pp. 805–12.
13. M. Sharma, H.A. Dabkowska, and N. Dogan: *Steel Res. Int.*, 2019, vol. 90, p. 1800367.
14. Z. Ren, X. Hu, X. Hou, X. Xue, and K. Chou: *Int. J. Min. Met. Mater.*, 2014, vol. 21, pp. 345–52.
15. B. Ozturk: *Metall. Mater. Trans. B*, 1992, vol. 23B, pp. 523–26.
16. S.K. Michelic and C. Bernhard: *Scanning*, 2017, vol. 2017, pp. 1–14.
17. W. Wang, E. Gao, L. Zhou, L. Zhang, and H. Li: *J. Iron Steel Res. Int.*, 2019, vol. 26, pp. 335–64.
18. T. Mukongo, P.C. Pistorius, and A.M. Garbers-Craig: *Ironmak. Steelmak.*, 2004, vol. 31, pp. 135–43.
19. P. Rocabois, J. Lehmann, C. Gatellier, and J.P. Teres: *Ironmak. Steelmak.*, 2003, vol. 30, pp. 95–100.
20. O.K. Tokovoi and D.V. Shaburov: *Steel Transl.*, 2013, vol. 43, pp. 678–80.
21. Z. Chen, M. Li, X. Wang, S. He, and Q. Wang: *Metals*, 2019, vol. 9, pp. 635–50.
22. L. Zhou, J. Li, W. Wang, and I. Sohn: *Metall. Mater. Trans. B*, 2017, vol. 48B, pp. 1943–50.
23. W. Wang, J. Li, L. Zhou, and J. Yang: *Met. Mater. Int.*, 2016, vol. 22, pp. 700–06.

**Publisher's Note** Springer Nature remains neutral with regard to jurisdictional claims in published maps and institutional affiliations.